Analyst

Interdisciplinary detection science

www.rsc.org/analyst

Volume 136 | Number 6 | 21 March 2011 | Pages 1053–1264

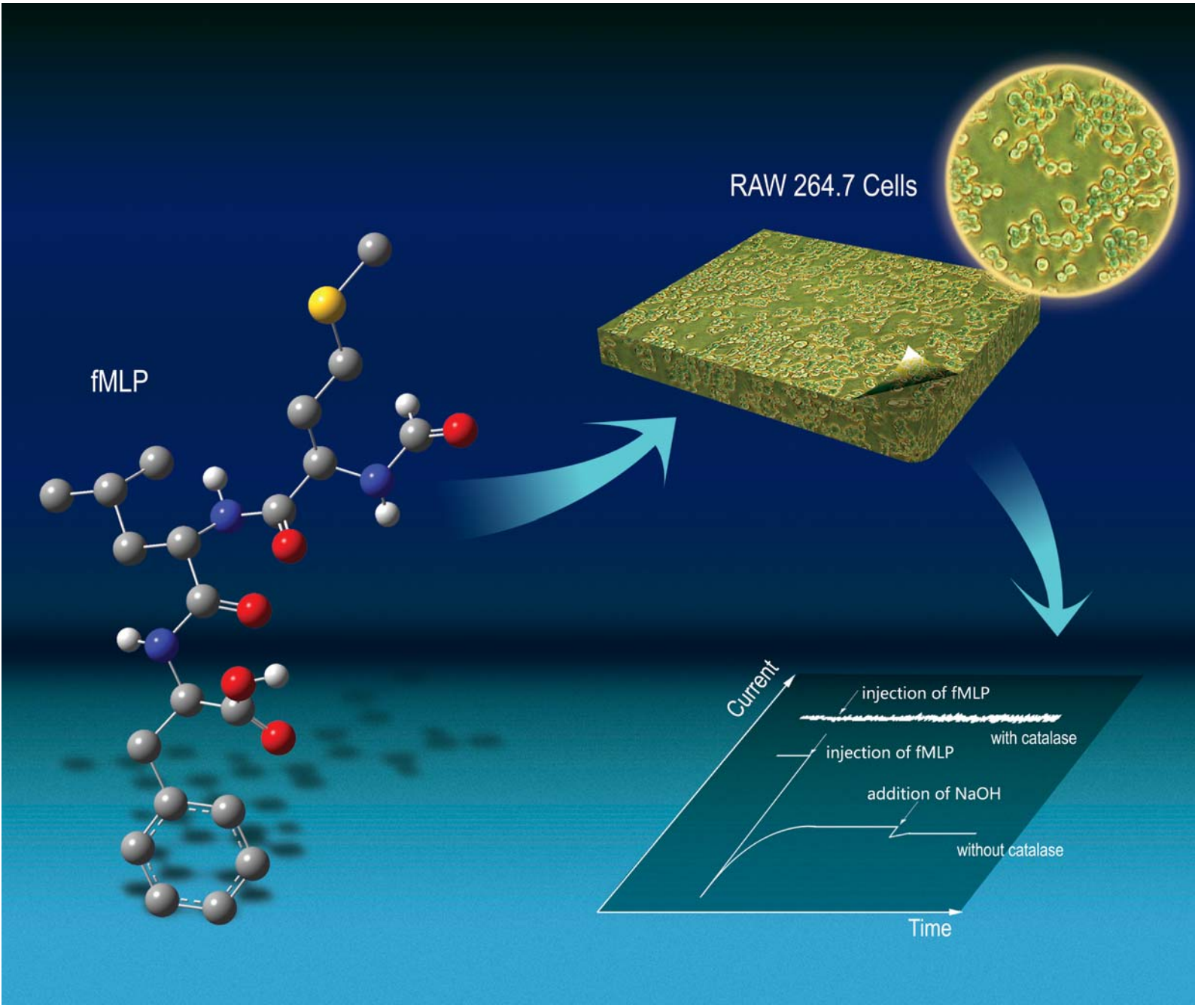

ISSN 0003-2654

HOT ARTICLE

Chenxin Cai *et al.*

Electrochemical detection of extracellular hydrogen peroxide released from RAW 264.7 murine macrophage cells based on horseradish peroxidase–hydroxyapatite nanohybrids

RSC Publishing

0003-2654(2011)136:6;1-H

Analyst

Dynamic Article Links

Cite this: *Analyst*, 2011, **136**, 1116

www.rsc.org/analyst

PAPER

Electrochemical detection of extracellular hydrogen peroxide released from RAW 264.7 murine macrophage cells based on horseradish peroxidase–hydroxyapatite nanohybrids†

Chunyun Li,[a] Hui Zhang,*[a] Ping Wu,[a] Zhunan Gong,[b] Guanglin Xu[b] and Chenxin Cai*[a]

Received 26th October 2010, Accepted 7th December 2010
DOI: 10.1039/c0an00825g

A new method developed for the reliable determination of extracellular and intracellular H_2O_2 is very useful for gaining a full understanding of the role that H_2O_2 plays in pathology and physiology, and the relationship between H_2O_2 and environmental stresses and lipid peroxidation. This work developed and validated an electrochemical approach for the determination of extracellular H_2O_2 released from RAW 264.7 murine macrophage cells. This approach is based on the electrocatalytic reduction of the released H_2O_2 at the biosensor of HRP–HAP/GC, which was fabricated by depositing the horseradish peroxidase–hydroxyapatite (HRP–HAP) nanohybrids on a glassy carbon (GC, 3 mm in diameter) electrode. The biosensor exhibited a rapid response (less than 2 s), a low detection limit (0.1 ± 0.02 μM), a wide linear range (5 μM to 0.82 mM), as well as good stability and repeatability. In addition, the common interfering species, such as uric acid (UA), ascorbic acid (AA), glucose, and 3,4-dihydroxyphenylacetic acid (DOPAC), *etc.*, did not cause any interference due to the use of a low operating potential (−400 mV, *versus* SCE). Therefore, this work has demonstrated a simple and effective sensing platform for the detection of extracellular H_2O_2 released from cells such as RAW 264.7 cells, which has potential utility to bioelectroanalytical chemistry, cellular biology, and pathophysiology.

Introduction

Reactive oxygen species (ROS), including hydroxyl radicals ($^{\bullet}OH$), superoxide anions ($O_2^{\bullet-}$), peroxynitrite ($ONOO^-$), and hydrogen peroxide (H_2O_2), *etc.*, are ubiquitous in life and death processes of cells.[1] They are considered as the mediators of the biochemistry of cellular pathology and may be involved in a number of pathological events connected with lipid peroxidation,[2] organ injury,[3] DNA damage,[4] tumor promotion,[4] *etc.* Under normal metabolic conditions, ROS are produced at a rate matching the capacity of tissue to catabolize them. When their production exceeds the body's natural ability to deal with the potentially cytotoxic species, a variety of pathological conditions may result, including cancer, stroke, and neurodegeneration,[5,6] *etc.* Among the ROS, H_2O_2 is the most stable species, and has captured the interest of many researchers since it can exert diverse pathological and/or physiological effects in living systems and participate in the physiological processes in a concentration-dependent manner.[7–10] At low concentrations, it serves as a messenger in normal cellular signal transduction and plays an important role in protecting the living body.[7–9] Whereas at high concentrations, it can damage cellular constituents and cause various types of diseases.[10] Therefore, the quantitative determination of intracellular and extracellular H_2O_2 could lead to a better understanding of the clinical consequences of the enhancement in H_2O_2 concentration as well assisting in studies designed to elucidate the biological effect of H_2O_2 in cells.[11]

Various techniques have been developed for the analysis of H_2O_2 in a biological environment, including electrochemical methods,[12,13] chemiluminescence,[14,15] capillary electrophoresis chemiluminescence (CE-CL),[16] microchip electrophoresis coupled with chemiluminescence detection (MCE-CL),[17] or with laser-induced fluorescence detection (MCE-LIF),[11,18] fluorescence,[19–21] *etc.* Among these methods, the electrochemical approach has attracted significant attention and has become an attractive method for *in vivo* and *ex vivo* biological application, including continuous *in vivo* monitoring, measurement of analytes in extremely small volumes, monitoring of localized events because of their high sensitivity, low cost, rapid response, compatibility for miniaturization, and compatibility with microfabrication technology.[12,13,22]

[a]*Jiangsu Key Laboratory of New Power Batteries, Jiangsu Key Laboratory of Biofunctional Materials, Laboratory of Electrochemistry, College of Chemistry and Materials Science, Nanjing Normal University, Nanjing 210097, P. R. China*

[b]*College of Life Science, Nanjing Normal University, Nanjing 210046, P. R. China. E-mail: cxcai@njnu.edu.cn*

† Electronic supplementary information (ESI) available. See DOI: 10.1039/c0an00825g

Electrochemical approaches for the determination of H_2O_2 are often based on the direct oxidation of H_2O_2 on the electrode surface. However, the oxidation of H_2O_2 usually requires a relatively high positive potential (usually over +0.6 V *versus* SCE). Many other electroactive species coexisting in the biological fluids can also be oxidized at such a high potential, and their electrochemical signals thus severely affect the selectivity of the assay. Therefore, interference elimination represents a main task to be solved for this type of method. The interference can be partially overcome by coating the electrode with a membrane impermeable to interfering species[23] or oxidizing the interfering species before they reach the surface of the electrode.[24] However, coating with polymeric films leads to lower signals and longer response times due to the additional diffusion barrier, whereas using electrochemical preoxidation displays a risk of oxidizing the substrate of interest. To eliminate this risk, the oxidation of the interfering species can be accomplished by enzymatic preoxidation, which is achieved either by incorporating specific enzymes in the electrode configuration or immobilizing them in reactors, thus complicating the electrode fabrication procedures.

Alternatively, H_2O_2 can be electrochemically detected based on its reduction because the electrochemical reduction of H_2O_2 that occurred at a relatively negative potential does not give rise to the interference from those common interfering species.[22a,25] It has been reported that the heme proteins or enzymes can catalyze the reduction of H_2O_2 with high sensitivity and selectivity.[26–31] Therefore, H_2O_2 biosensors can be developed by immobilizing heme proteins on the surface of the suitable materials or directly on the electrode surface. To simplify the fabrication procedures and enhance the efficiency of the biosensor, it is highly desirable to synthesize the stable and biocompatible materials for immobilizing the heme proteins or enzymes. This work reports a horseradish peroxidase (HRP)-based H_2O_2 biosensor based on the reduction of H_2O_2 with the use of hydroxyapatite (HAP) nanostructures as the enzyme immobilization matrix. HAP adopts the ideal composition $Ca_{10}(PO_4)_6(OH)_2$ that is thermally stable and contains both acid and base sites, including hydroxyl-enriched channels.[32] These structural features allow HAP to have good biological properties such as non-toxicity, and good biocompatibility,[33] *etc*. The preparation and characteristics of the biosensor are presented. The developed biosensor exhibits facile fabrication, good performance, fast response, accepted stability and reproducibility, and low detection limit. Moreover, the biosensor can be used for the determination of the extracellular H_2O_2 released by RAW 264.7 murine macrophage cells. Our goal is not only to design a novel biosensing platform but also to present a new approach for the determination of extracellular and intracellular H_2O_2, which has potential utility to bioelectroanalytical chemistry, cellular biology, pathophysiology, *etc*.

Experimental

Chemicals

Horseradish peroxidase (HRP, E.C. 1.11.1.7, Type VI, MW ≈ 44 000, RZ ≈ 3.0, lyophilized powder, 250–330 U mg^{-1}, Sigma), catalase (E.C. 1.11.1.6, from bovine liver, lyophilized powder, 2000–5000 U mg^{-1}, Sigma), *N*-formylmethionyl-leucyl-phenylalanine (fMLP, Sigma), and 3-(4,5-dimethyl-2-thiazolyl)-2,5-diphenyl-2*H*-tetrazolium bromide (MTT, Sigma) were used without further purification. Glucose, 3,4-dihydroxyphenylacetic acid (DOPAC), ascorbic acid (AA), uric acid (UA), and dimethyl sulfoxide (DMSO) were purchased from Shanghai Chemical Reagent Co. Ltd. (Shanghai, China) and used as received. Solutions of H_2O_2 were freshly diluted from the 30% solution, and their concentrations were determined using a standard $KMnO_4$ solution. 0.1 M phosphate buffer solution (PBS, pH 7.4) was employed as the supporting electrolyte. Other chemicals were of analytical grade. All solutions were prepared with double distilled water.

Apparatus

Transmission electron microscope (TEM) images were obtained on a Hitachi H-7650 microscope. X-Ray diffraction (XRD) patterns were performed using a Rigaku/Max-3A X-ray diffractometer with Cu-Kα radiation ($\lambda = 0.15418$ nm). The FT-IR spectra were recorded on a Nexus 670 FT-IR spectrophotometer (Nicolet Instruments) using a KBr disk at a resolution of 4 cm^{-1}. UV-vis spectra were recorded using a Cary 5000 UV-vis-NIR spectrophotometer (Varian, USA). The Zeta potential (ζ) value of the prepared HAP nanostructures was measured using a particle size analyzer (Zetasizer Nano, Malvern, UK). The image of RAW 264.7 murine macrophage cells on the electrode surface was recorded with a BX41-32P02 microscope (Olympus).

The electrochemical experiments were carried out with a CHI 760C electrochemical workstation (CH Instruments). A two-compartment three-electrode cell with the sample volume of 10 mL was employed. A coiled Pt wire and a saturated calomel electrode (SCE) were used as the counter electrode and the reference electrode, respectively. Buffers were purged with high purity nitrogen for at least 30 min prior to experiments and the nitrogen environment was then kept over the solution to prevent oxygen from reaching the solution. Amperometric measurements were performed under a constant potential of −400 mV (*versus* SCE). The solution was continuously stirred using a magnetic bar at a rate of 250 rpm. All electrochemical experiments were performed at room temperature (22 ± 1 °C).

Synthesis of HAP nanostructures

The HAP nanostructures were synthesized by a chemical precipitation method according to the reported procedures with a minor modification.[34] The details of synthesizing are described in the Supplementary Information.†

Assembly of HRP and fabrication of the HRP–HAP/GC electrode

Several experimental parameters were optimized to obtain the best voltammetric response. For the immobilization of HRP, HAP (10 mg) was dispersed into HRP solution (2 mL, 5 mg mL^{-1} in pH 7.4 PBS) by continuously stirring at 4 °C for 2 h. HRP was assembled on the surface of the negatively charged HAP *via* electrostatic interaction. After that, the mixture was centrifuged and the HRP–HAP nanohybrids were collected by removing the supernatant. The nanohybrids were thoroughly washed with PBS to remove the loosely assembled enzyme molecules.

To fabricate the HRP–HAP/GC electrode, the HRP–HAP nanohybrid was dispersed into PBS (pH 7.4) to form a homogeneous suspension (5 mg mL^{-1}). Then, the suspension (4 μL) was cast onto the surface of the glassy carbon (GC, 3 mm in diameter, CH Instruments) electrode with a microsyringe, and the solvent was allowed to evaporate at ambient temperature before use. The HRP–HAP/GC electrode was stored at 4 °C when not in use.

By similar procedures, the HAP/GC and HRP/GC electrodes were also fabricated, and their electrocatalytic characteristics were compared with those of the HRP–HAP/GC electrode.

Cell culture, immobilization, and lysate preparation

The RAW 264.7 murine macrophage cells were grown at 37 °C in DMEM (Dulbecco's Modified Eagle Medium) supplemented with 10% (v/v) fetal bovine serum (FBS), 100 U mL^{-1} penicillin, and 100 μg mL^{-1} streptomycin in a 5% CO_2 environment. After growing to 90% confluence, the cells were then washed three times with PBS (0.145 M NaCl, 1.9 mM NaH_2PO_4, 8.1 mM K_2HPO_4, pH 7.4) and the cell number was estimated by a hemocytometer.

For the immobilization of cells on the electrode surface, the cells were suspended in PBS to obtain a homogeneous cell suspension with the final concentration of *ca.* 3.0×10^6 cells mL^{-1}. 5 μL of the suspension was dropped onto the surface of the HRP–HAP/GC electrode and then the electrode was incubated at 37 °C for 2 h to achieve cell immobilization. Therefore, about 1.5×10^4 cells were immobilized on the surface of the electrode. The immobilization of cells on the surface of the electrode may alter the bioactivities of the cells, thus, MTT assay, which is a colorimetric assay for assessing the viability of cells,[35] was conducted on the immobilized cells. After the cells were immobilized on the electrode surface, 20 μL of MTT solution (5 mg mL^{-1} in PBS, pH 7.4) were added onto the electrode surface and incubated for 4 h at 37 °C. During the incubation, MTT (a yellow tetrazole) is reduced to insoluble purple formazan by mitochondrial reductase in living cells.[35] Afterward, the product was dissolved into a vial from the electrode surface with 200 μL DMSO, and the volume was adjusted to 2 mL by adding PBS. The absorbance of this colored solution at 570 nm was recorded. For comparison, MTT assay was also performed with the cells before immobilization. 5 μL of the cell suspension (3.0×10^6 cells mL^{-1}) was put into a vial, 20 μL of MTT solution were added and incubated for 4 h, and 200 μL DMSO were added onto the vial for dissolving the formazan product. Finally, after the volume of solution was fixed to 2 mL, the absorbance of the solution at 570 nm was measured and compared with that of the immobilized cells. The results indicated that the absorbance is almost identical with that for the immobilized cells (not shown here), suggesting that immobilization of the cells on the electrode surface does not change the bioactivities of the cells due to the good biocompatibility of HAP.

The concentrations of H_2O_2 in RAW 264.7 murine macrophage cells were measured using the developed HRP–HAP/GC electrode. Cells were lysed with 0.3 M KOH, and then the lysate was sonicated. The samples were centrifuged at 18 000 rpm for 30 min and the supernatant was filtered through a 0.22 μm Nylon filter. The concentration of H_2O_2 in the filtrate was measured by recording the response currents of H_2O_2 reduction at the HRP–HAP/GC electrode under a constant potential (−400 mV, *versus* SCE).

To study the effects of fMLP, which is a strong chemoattractant and induces adherence, degranulation and production of tissue-destructive oxygen-derived free radicals in macrophage cells, on the H_2O_2 generation in cells, fMLP (the final concentration is 0.3 μM) was added to the cell suspension to induce H_2O_2 generation. After treatment of the cells for various times, the cells were lysed, centrifuged, and the supernatant was filtered. The concentration of H_2O_2 was analyzed. The effects of the concentration of fMLP on the H_2O_2 generation in the cells were also studied. Various concentrations of fMLP (the final concentration ranges from 0.1 to 0.5 μM) were injected into the cell suspension to induce the generation of H_2O_2 for 1 h, and the concentration of H_2O_2 was evaluated with use of the developed electrode.

The release process of H_2O_2 by the cell was studied by recording the reduction response of H_2O_2 released from the cells, which were immobilized on the surface of the HRP–HAP/GC electrode. After a steady state background was attained, fMLP solution (the final concentration is 0.3 μM) was injected into the buffer, and the release of H_2O_2 was monitored by recording the change of the reduction current of H_2O_2 at the electrode with time. The measurements were performed under the physiological pH and temperature (pH 7.4 and 37 °C).

Results and discussion

Characterization of HAP nanostructures and HRP–HAP nanohybrids

XRD analysis was used to examine the crystal structure and phase purity of the as-synthesized HAP nanostructures. The obtained XRD patterns (Fig. S1†) are in good agreement with those of the reference patterns for hexagonal phase HAP (JCPDS 09-0432). The lattice parameters (a and c) for hexagonal phase HAP nanostructures can be calculated to be $a = 9.421 \pm 0.022$, and $c = 6.886 \pm 0.011$ Å, respectively, which are close to those reported in JCPDS 09-0432 ($a = 9.418$ and $c = 6.884$ Å). These results confirm that the as-synthesized HAP nanostructures have a highly crystalline hexagonal phase, and no impurity phases could be found from the XRD patterns. The results of IR spectra also demonstrate the successful preparation of HAP nanostructures (Fig. S2†).

The TEM image indicates that the HAP nanostructures have a needle-like morphology with an average size of 20–25 nm in width and 160–180 nm in length (Fig. 1). The HAP nanostructures have a rough surface characteristic. This feature is very useful for the nanostructures being used for substrate to immobilize the enzymes because the rough surface can significantly enhance the enzymes loading and therefore, increasing the electrochemical response.

Zeta potential (ζ) analysis indicates that HAP nanostructures have a net negative surface charge in PBS (pH 7.4) since the value of ζ for the nanostructures is *ca.* –(20 ± 2) mV. As the isoelectric point of HRP is ~8.9,[36] HRP is positively charged in pH 7.4 PBS. Therefore, HRP could easily be assembled on the HAP surface by electrostatic interaction.

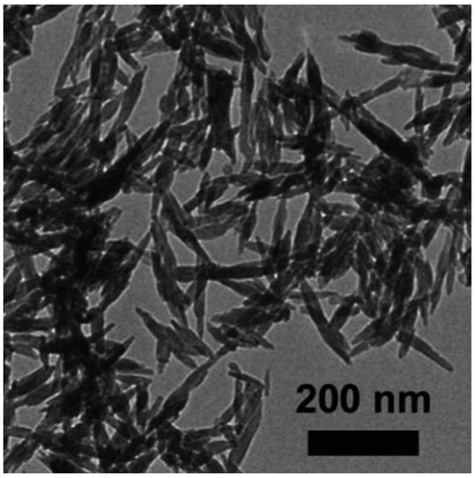

Fig. 1 Typical TEM image of HAP nanostructures.

The assembly of HRP on the surface of HAP can be verified by UV-vis spectroscopic characterization. The UV-vis spectrum of HRP–HAP shows the Soret band at 402 nm (curve c, Fig. 2), indicative of the successful assembly of HRP on the HAP nanostructures. The features of this peak are identical with those of natural HRP dissolving in solution (402 nm, curve b, Fig. 2), suggesting that no significant denaturation occurred to the protein after being assembled onto the surface of the HAP nanostructures. This conclusion is further supported by the IR spectra presented in Fig. S2.† These results also show good biocompatibility of the nanostructures.

SEM images can provide additional information on the assembly of HRP on the surface of the HAP nanostructures. The image indicates that the needle-like nanostructures distribute almost uniformly on the entire surface of the GC electrode, exhibiting a special three-dimensional porous structure (Fig. 3a), which can significantly increase the effective surface of the electrode for loading biomolecules. The morphology of the HRP–HAP nanohybrids presented in Fig. 3b shows that the size of the HRP–HAP nanohybrids is slightly larger than that of HAP nanostructures, indicating the assembly of HRP on the surface of HAP. Moreover, the morphology of HRP–HAP nanohybrids on the electrode surface has a similar three-dimensional structure to that of HAP nanostructures. Such a structure is expected to be

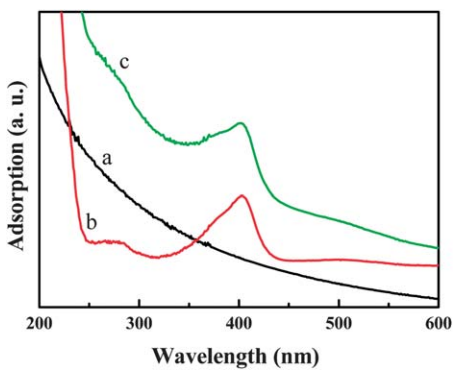

Fig. 2 UV-vis spectra of HAP nanostructures (a), HRP in solution (0.5 mg mL^{-1}, b), and HRP–HAP nanohybrids (c).

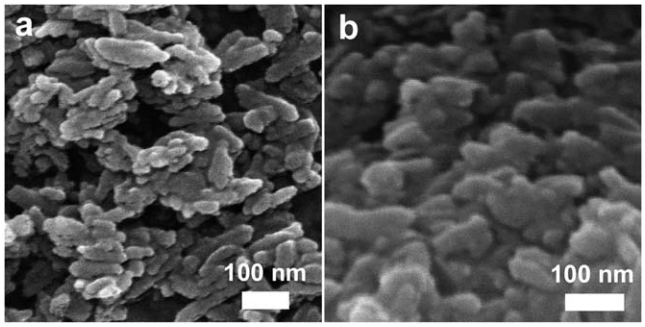

Fig. 3 SEM images of HAP nanostructures (a) and HRP–HAP nanohybrids (b).

very attractive for the detection of substrates because each of the HRP–HAP nanohybrids is fully and easily accessible to substrates, and thus can be used as an electrochemical sensing unit, yielding a high signal-to-noise ratio for electrochemical determination.

Electrocatalytic reduction of H_2O_2 at the HRP–HAP/GC electrode

The aim of this work is to develop a biosensor for analyzing the level of H_2O_2 released from cells. To evaluate the possibility of the HRP–HAP/GC electrode being used for this purpose, the voltammetric responses of the electrode in PBS with and without H_2O_2 are recorded. In the absence of H_2O_2, the voltammetric response of the electrode shows a pair of well-defined and nearly symmetrical redox peaks with E_{pc} and E_{pa} of *ca.* −400 and −340 mV (at 100 mV s^{-1}), respectively (curve a, panel A in Fig. 4), which can be ascribed to the direct electron transfer (DET) reaction of HRP assembled on the surface of the HAP nanostructures (please refer to detailed analysis presented in the

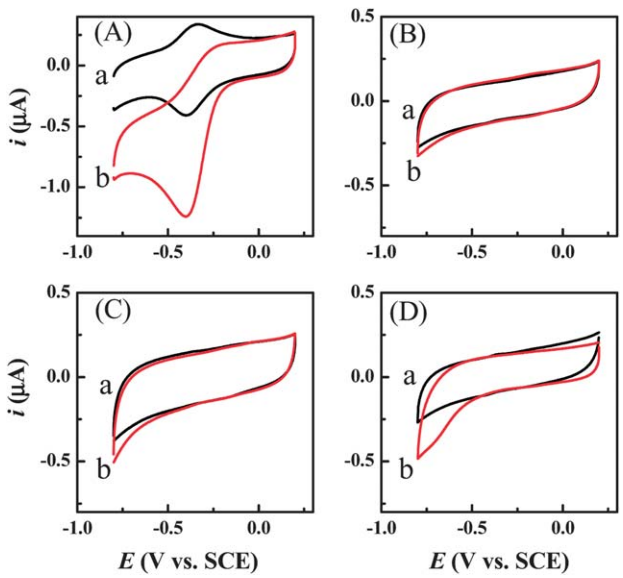

Fig. 4 Voltammetric responses of the HRP–HAP/GC (A), bare GC (B), HAP/GC (C), and HRP/GC electrodes (D) in N_2-saturated PBS (0.1 M, pH 7.4) with (curve b) and without (curve a) 0.2 mM H_2O_2. Scan rate was 100 mV s^{-1}.

Supplementary Information†). The separation of peak potentials, ΔE_p, is 60 mV, indicating that HAP can facilitate the effective DET between HRP and the electrode surface in spite of the large molecular structure of HRP. The formal potential ($E^{0\prime}$) is estimated to be −370 mV, which is close to those previous reports for HRP trapped in polymer films, such as poly(ethylene glycol) (−370 mV)[37] and tributylmethylphosphonium chloride polymer (−377 ± 5 mV),[38] and also similar to that obtained by adsorbing HRP on the surface of TiO_2 (−350 mV).[39] These results also show that HRP assembled on the surface of HAP nanostructures can keep its natural structure. The conclusion is in good agreement with that obtained from UV-vis and IR spectra.

Upon addition of 0.2 mM H_2O_2, the shape of the cyclic voltammogram of the electrode changes significantly, being characterized by a large cathodic peak at *ca.* −400 mV (curve b, panel A) and complete disappearance of the anodic peak. The increase of H_2O_2 concentration leads to the enhancement of the cathodic current. These characteristics are the typical features of electrocatalytic reactions. The reduction of H_2O_2 starts at a potential of *ca.* −100 mV, and the observed reduction current increases quite rapidly during negative potential scanning and reaches the highest catalytic current at *ca.* −400 mV. The onset potential is 300 mV more positive than where the reduction peak actually appears. The results presented in panels B, C, and D (Fig. 4) show that the presence of H_2O_2 in PBS does not affect the voltammetric features of the bare GC, HAP/GC, and HRP/GC electrodes except that only a weak reduction current can be observed at the potential more negative than −520 mV at the HRP/GC electrode (panel D), demonstrating that bare GC, HAP, or HRP immobilized on the GC electrode surface does not have any appreciable electrocatalytic activity toward the reduction of H_2O_2. Therefore, it can be concluded that HRP–HAP nanohybrids present a good electrocatalyst for the reduction of H_2O_2. All these features indicate that HRP assembled on the HAP nanostructures retains its intrinsic and good electrocatalytic activities towards its substrates. The biocompatibility of HAP enables the nanostructure to become a good biosensing platform for realizing direct electrochemistry and electrocatalysis of heme-containing proteins/enzymes.

The response of the biosensor usually depends on the detection potential, and this work optimized the parameter to achieve the highest sensitivity and avoid the electrochemical interfering species. The response increases with the detection potential from −100 to −400 mV (*versus* SCE) and then reaches a plateau at more negative potentials (not shown here). Thus, a detection potential of −400 mV is selected. Fig. 5 depicts the typical steady state amperometric response of the HRP–HAP/GC electrode to the successive addition of H_2O_2 in PBS (pH 7.4) solution at a detection potential of −400 mV. Immediately after the addition of H_2O_2, the response increases and reaches 95% of the steady-state value within *ca.* 2 s. The response time is much shorter than *ca.* 35, 15, and 8 s obtained at the HAP-Nafion-silica sonogel-carbon composite electrode,[40] HRP/Au colloid/cysteamine-modified electrode,[41] and HRP-Au NPs-silk fibroin/GC electrode,[42] respectively. These results suggest that the electrode responds rapidly to the change of the substrate concentration due to the fast diffusion of the substrate in the HAP porous film.[43] The electrode linearly responds to H_2O_2 concentration at lower

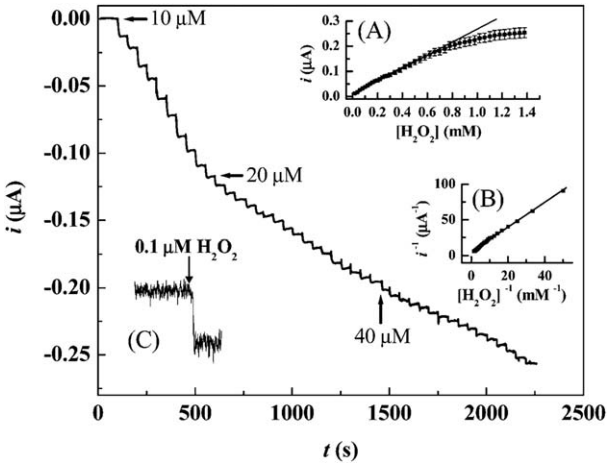

Fig. 5 Amperometric responses of the HRP–HAP/GC electrode to the successive addition of H_2O_2 in PBS (0.1 M, pH 7.4) at an applied potential of −400 mV. The insets show the dependence of the response of the electrode on H_2O_2 concentration under the optimal conditions (inset A), the Lineweaver–Burk plot (inset B), and the relationship of the signal-to-noise ratio at S/N of 3 (inset C).

concentrations and attains saturation levels at higher concentrations (inset A, Fig. 5), representing a typical Michaelis–Menten enzymatic reaction characteristic. The response displays a good linear range from 5 μM to 0.82 mM with a correlation coefficient of 0.998. The detection limit is estimated to be *ca.* (0.1 ± 0.02) μM (at a signal/noise of 3, inset C, Fig. 5), which is comparable to that obtained at the HRP-TiO_2 nanotube arrays modified electrode (0.1 μM),[44] but much lower than those obtained at the HAP-α-zirconium phosphate/GC electrode (1.2 μM),[45] HRP-nano-Au-carbon ceramic electrode (6.1 μM),[46] and HRP-DNA/GC electrode (25 μM).[47] The apparent Michaelis–Menten constant (K_M^{app}) is estimated to be (0.47 ± 0.08) mM from the Lineweaver–Burk plot (inset B of Fig. 5). The value of K_M^{app} is lower than those reported at the HRP-chitosan-silica sol–gel/Pt electrode (0.93 mM),[48] HRP-sodium alginate-polyvinyl butyral/gold electrode (1.38 mM),[49] HRP/Nafion-methylene-green/GC electrode (2.1 mM),[50] and sol–gel-derived ceramic-carbon nanotube nanocomposite film modified electrode (23.85 mM),[51] indicating the good biocompatibility of the HAP nanostructures. The linear range is much wider than those obtained at the HRP-AuNP-TiO_2 nanotube arrays modified electrode (5 μM to 0.4 mM),[52] HRP-mesoporous silica hollow sphere-Nafion/GC electrode (3.9 μM to 0.14 mM),[53] and HAP-Nafion-silica sonogel-carbon composite electrode (4 μM to 0.1 mM).[40] These results suggest that HAP nanostructures can be used as a platform for the development of enzyme-based amperometric biosensors for H_2O_2 determination.

Different aspects regarding the characteristics of the biosensor are evaluated. The RSD (relative standard deviation) is ∼2.2% estimated from slopes of calibration plots for 7 different and freshly prepared electrodes, revealing an acceptable repeatability in the construction of the biosensor. The assay precision of the biosensor was examined by 10 determinations at an H_2O_2 concentration of 0.5 mM. An RSD of ∼2.8% is obtained. Also, the long-term stability of the biosensor is considered by amperometric measurements. When the electrode was not in use, it was

stored in buffer at 4 °C. Its response to 0.5 mM H_2O_2 was recorded at 2-day intervals. The response reveals that the electrode maintains *ca.* 90% of its initial current response to H_2O_2 even after 2 weeks. Another attractive feature of the biosensor is that the response remains almost unchanged even after it is under extended polarization at −400 mV for 4 h in a stirred solution of 0.5 mM H_2O_2. This means that the biosensor can be used as a stable probe for H_2O_2 detection. The high stability can be attributed to the capability of the HAP nanostructures assembling HRP molecules and retaining their biological activities. This improved stability may also be attributed to the special structure of the HRP–HAP, which is beneficial for the substrates getting access to the enzyme molecules.

Another advantage of the developed biosensor is that the common interfering species such as glucose, AA, UA, DOPAC, *etc.* result in negligible signals compared to that of H_2O_2 (Fig. S3†) due to the use of a low operating potential in the detection. Therefore, highly selective response to H_2O_2 is obtained without the use of a perm-selective membrane or enzymatic preoxidation. These results indicate the suitability of the proposed biosensor to practical applications.

Determination of H_2O_2 released from cells

The developed HRP–HAP/GC electrode was used for measuring the concentration of H_2O_2 in RAW 264.7 murine macrophage cells. The results indicated that the H_2O_2 concentration in the cell is *ca.* 8.0 ± 0.4 nM (Fig. 6), which is in agreement with that reported previously based on fluorescence method,[21] suggesting that the developed electrode can be used for determination of the concentration of H_2O_2 in cells. The developed method was also used to measure H_2O_2 in RAW 264.7 murine macrophage cells in response to fMLP treatment since fMLP is known to induce the generation of H_2O_2 in RAW 264.7 murine macrophage cells.[54] The cells were exposed to fMLP at concentrations ranging from 0.1 to 0.5 μM for 30 min and then lysed with 0.3 M KOH. Panel A in Fig. 6 depicts the dependence of the amount of H_2O_2 generated in the cell on the fMLP loading. The amount of H_2O_2 in RAW 264.7 murine macrophage cell is significantly increased with the enhancement of the fMLP concentration, and it reaches the highest value (*ca.* 17 ± 0.8 nM) at an fMLP concentration of 0.3 μM. After that, the concentration of H_2O_2 generated by the cells decreases with the enhancement of the fMLP loading. This may be because an extra high concentration of H_2O_2 induced by the high loading of fMLP can damage the lipid membrane of the cells and even cause cell death.[55] This result leads to the decrease in the amount of released H_2O_2. Therefore, a concentration of 0.3 μM for fMLP is selected for further experiments.

The amount of H_2O_2 generated in RAW 264.7 murine macrophage cells is also affected by the time of fMLP treatment. Panel B in Fig. 6 depicts the time course experimental results with fMLP loading at a constant concentration of 0.3 μM for fMLP. The value of H_2O_2 in RAW 264.7 murine macrophage cells is significantly increased after treatment with 0.3 μM fMLP. The concentration of H_2O_2 increases with the increase of the inducement time and the highest value is attained at the time of 30 min. Afterwards the concentration decreases gradually and reaches a relatively stable value (*ca.* 13 nM) at 3 h.

The released process of H_2O_2 by the RAW 264.7 cells was also evaluated using the developed electrode. The cells (*ca.* 1.5×10^4 cells) were immobilized on the surface of the HRP–HAP/GC electrode (the image of the cells on the electrode surface is depicted in panel A of Fig. 7, where the size of the cell can be estimated to *ca.* 20 μm in diameter). After the steady-state background was attained, fMLP was introduced into the solution (the final concentration is 0.3 μM), and the release of H_2O_2 was monitored by recording the change of the response of the electrode. The response of the electrode increases immediately after the injection of fMLP (curve a, panel B in Fig. 7), indicative of the fast release of H_2O_2 from the cells after being treated with

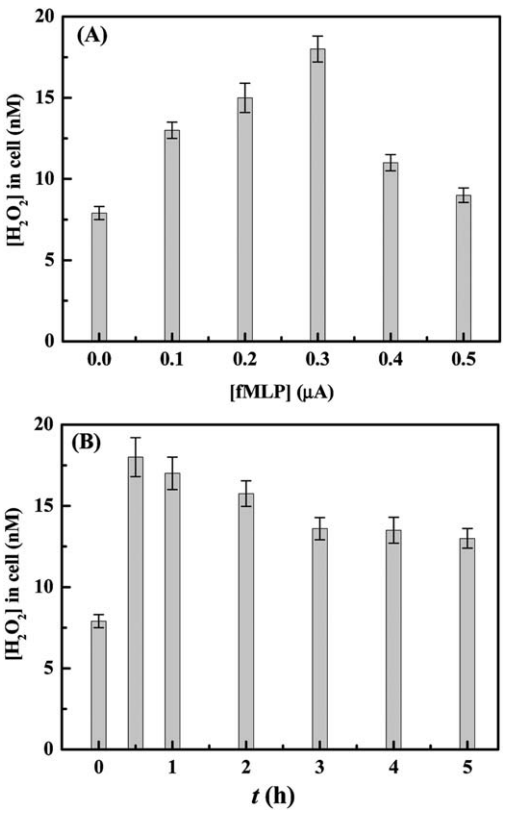

Fig. 6 Dependence of the amount of H_2O_2 generated in RAW264.7 murine macrophage cells on the concentration of fMLP at a fixed treatment time of 30 min (A), and on the treatment time at a fixed fMLP concentration of 0.3 μM (B).

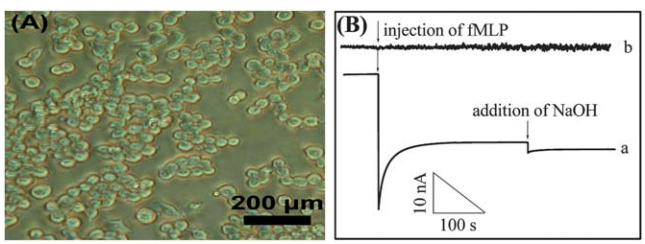

Fig. 7 (A) Image of the cells on the electrode surface; and (B) typical amperometric responses of the HRP–HAP/GC electrode for the reduction of H_2O_2 released from RAW264.7 murine macrophage cells induced by fMLP (0.3 μM) with (curve b) and without (curve a) addition of 50 μL of catalase (300 U mL^{-1}). The electrode was biased at a constant potential of −400 mV (*versus* SCE).

fMLP. After a stable response is reached, addition of NaOH solution to the system (the final concentration is 0.3 M) results in an enhancement in the response of the electrode (curve a, panel B in Fig. 7). This is because when the cells are lysed by the injection of NaOH into the solution, more H_2O_2 is released from the cells, leading to the increase of the reduction currents for H_2O_2 reduction at the electrode. To verify that the response depicted in curve a (Fig. 7) is only due to the response of the released H_2O_2 from RAW 264.7 cells, 50 μL of catalase solution (500 U mL^{-1}), which was known as a selective scavenger of H_2O_2, were injected into the solution before the addition of fMLP. The response of H_2O_2 at the electrode disappears (curve b, panel B in Fig. 7) since the released H_2O_2 was scavenged by catalase, demonstrating that the addition of fMLP can only induce the release of H_2O_2 from RAW 264.7 cells and cannot lead to the release of O_2. Otherwise, the response of the electrocatalytic reduction of O_2 at the electrode should be observed because catalase cannot scavenge O_2. Therefore, the proposed method could be used for studying the intracellular kinetics of H_2O_2 generation. These observations substantially demonstrate that the developed method represents a new biosensing platform for the reliable determination of extracellular and intracellular H_2O_2 and could be potentially useful for further physiological and pathological studies.

Conclusions

A new amperometric H_2O_2 biosensor based on the immobilization of HRP on the surface of HAP nanostructures has been developed. The biosensor exhibited a fast response, a broad linear range, a low detection limit with satisfactory stability and repeatability and would have great potential application in the determination of H_2O_2 concentration in both intracellular and extracellular samples. The fabrication method of the biosensor has many advantages such as ease of fabrication, enhanced electrocatalysis, efficiently preserving the activity of enzyme molecules, and effective discrimination to the common interfering species.

Acknowledgements

This work is supported by the National Natural Science Foundation of China (20773067, 20833006, and 20905036), the Foundation of the Jiangsu Education Committee (09KJA150001, 09KJB150006, and 10KJB150009), and Priming Scientific Research Foundation for Advanced Talents in Nanjing Normal University (2009103XGQ0064).

References

1 T. Finkel and N. J. Holbrook, *Nature*, 2000, **408**, 239–247.
2 A. Sevanian and P. Hochstein, *Annu. Rev. Nutr.*, 1985, **5**, 365–390.
3 R. M. Tate and J. E. Repine, Repine, Phagocytes, Oxygen Radicals, and Lung Injury, in *Free Radicals in Biology*, ed. W. A. Pryor, Academic Press, New York, 1984, p. 199.
4 W. Troll and R. Wiesner, *Annu. Rev. Pharmacol. Toxicol.*, 1985, **25**, 509–528.
5 F. van Lente, *Anal. Chem.*, 1993, **65**, 374R–377R.
6 B. Halliwell and J. M. C. Gutteridge, *Arch. Biochem. Biophys.*, 1986, **246**, 501–514.
7 S. G. Rhee, *Science*, 2006, **312**, 1882–1883.
8 T. Finkel, *Curr. Opin. Cell Biol.*, 2003, **15**, 247–254.
9 J. R. Stone and S. Yang, *Antioxid. Redox Signaling*, 2006, **8**, 243–270.
10 J. R. Williamson, K. Chang, M. Frangos, K. S. Hasan, Y. Ido, T. Kawamura, J. R. Nyengaard, M. van den Enden, C. Kilo and R. G. Tilton, *Diabetes*, 1993, **42**, 801–813.
11 H. M. Li, Q. L. Li, X. Wang, K. H. Xu, Z. Z. Chen, X. C. Gong, X. Liu, L. L. Tong and B. Tang, *Anal. Chem.*, 2009, **81**, 2193–2198.
12 Y. P. Luo, H. Q. Liu, Q. Rui and Y. Tian, *Anal. Chem.*, 2009, **81**, 3035–3041.
13 X. G. Li, Y. Liu, A. W. Zhu, Y. P. Luo, Z. F. Deng and Y. Tian, *Anal. Chem.*, 2010, **82**, 6512–6518.
14 C. Lu, G. Q. Song and J. M. Lin, *TrAC, Trends Anal. Chem.*, 2006, **25**, 985–995.
15 C. D. Fike, J. C. Slaughter, M. R. Kaplowitz, Y. Zhang and J. L. Aschner, *Am. J. Physiol.: Lung Cell. Mol. Phys.*, 2008, **295**, L881–L888.
16 J. H. Wang, L. M. Li, W. H. Huang and J. K. Cheng, *Anal. Chem.*, 2010, **82**, 5380–5383.
17 F. G. Ye, Y. Huang, Q. Xu, M. Shi and S. L. Zhao, *Electrophoresis*, 2010, **31**, 1630–1636.
18 X. C. Gong, Q. L. Li, K. H. Xu, X. Liu, H. M. Li, Z. Z. Chen, L. L. Tong, B. Tang and H. B. Zhong, *Electrophoresis*, 2009, **30**, 1983–1990.
19 B. C. Dickinson, C. Huynh and C. J. Chang, *J. Am. Chem. Soc.*, 2010, **132**, 5906–5915.
20 E. W. Miller, O. Tulyathan, E. Y. Isacoff and C. J. Chang, *Nat. Chem. Biol.*, 2007, **3**, 263–267.
21 G. Kim, Y. E. K. Lee, H. Xu, M. A. Philbert and R. Kopelman, *Anal. Chem.*, 2010, **82**, 2165–2169.
22 (*a*) D. X. Chen, Q. Wang, J. Jin, P. Wu, H. Wang, S. Q. Yu, H. Zhang and C. X. Cai, *Anal. Chem.*, 2010, **82**, 2448–2455; (*b*) X. M. Wu, Y. J. Hu, J. Jin, N. L. Zhou, P. Wu, H. Zhang and C. X. Cai, *Anal. Chem.*, 2010, **82**, 3588–3596; (*c*) G. S. Wilson and R. Gifford, *Biosens. Bioelectron.*, 2005, **20**, 2388–2403; (*d*) P. Rowiński, R. Bilewicz, M.-J. Stébé and R. Rogalska, *Anal. Chem.*, 2004, **76**, 283–291.
23 T. Yao, S. Suzuki, H. Nishino and T. Nakahara, *Electroanalysis*, 1995, **7**, 1114–1117.
24 E. Zilkha, A. Koshy, T. P. Obrenovitch, H. P. Bennetto and L. Symon, *Anal. Lett.*, 1994, **27**, 453–473.
25 P. Du, B. Zhou and C. X. Cai, *J. Electroanal. Chem.*, 2008, **614**, 149–56.
26 A. H. Liu, M. D. Wei, I. Honma and H. S. Zhou, *Anal. Chem.*, 2005, **77**, 8068–8074.
27 N. Li, J. Z. Xu, H. Yao, J. J. Zhu and H. Y. Chen, *J. Phys. Chem. B*, 2006, **110**, 11561–11565.
28 G. Y. Shi, Z. Y. Sun, M. C. Liu, L. Zhang, Y. Liu, Y. H. Qu and L. T. Jin, *Anal. Chem.*, 2007, **79**, 3581–3588.
29 H. Zhang, J. J. Xu and H. Y. Chen, *J. Phys. Chem. C*, 2007, **111**, 16564–16570.
30 J. B. Jia, B. Q. Wang, A. G. Wu, G. J. Cheng, Z. Li and S. J. Dong, *Anal. Chem.*, 2002, **74**, 2217–2223.
31 (*a*) P. X. Yuan, Y. Zhuo, Y. Q. Chai and H. X. Ju, *Electroanalysis*, 2008, **20**, 1839–1844; (*b*) C. X. Cai and J. Chen, *Acta Chim. Sin.*, 2004, **62**, 335–340; (*c*) Y. J. Yin, Y. F. Lü, P. Wu, P. Du, Y. M. Shi and C. X. Cai, *J. Solid State Electrochem.*, 2007, **11**, 390–397; (*d*) L. Meng, L. G. Yang, B. Zhou and C. X. Cai, *Nanotechnology*, 2009, **20**, 035502; (*e*) Y. F. Lü, Y. J. Yin, P. Wu and C. X. Cai, *Acta Phys.-Chim. Sin.*, 2007, **23**, 5–11; (*f*) Y. J. Yin, H. Zhang, P. Wu, B. Zhou and C. X. Cai, *Nanotechnology*, 2010, **21**, 425504.
32 J. Xu, T. White, P. Li, C. He and Y.-F. Han, *J. Am. Chem. Soc.*, 2010, **132**, 13172–13173.
33 M. Rouahi, E. Championb, O. Gallet, A. Jada and K. Anselme, *Colloids Surf. B: Biointerfaces*, 2006, **47**, 10–19.
34 J. Hong, X. Qiu, J. Sun, M. Deng, X. Chen and X. Jing, *Polymer*, 2004, **45**, 6699–6706.
35 T. Mosmann, *J. Immunol. Methods*, 1983, **65**, 55–63.
36 K. G. Welinder, *Eur. J. Biochem.*, 1979, **96**, 483–502.
37 Y. Xu, W. L. Peng, X. J. Liu and G. X. Li, *Biosens. Bioelectron.*, 2004, **20**, 533–537.
38 T. Ferri, A. Poscia and R. Santucci, *Biosens.Bioelectron.*, 1998, **44**, 177–181.
39 Y. Zhang, P. L. He and N. F. Hu, *Electrochim. Acta*, 2004, **49**, 1981–1988.
40 M. Elkaoutit, I. Naranjo-Rodriguez, M. Domínguez, M. P. Hernández-Artiga, D. Bellido-Milla and J. L. H. H. de Cisneros, *Electrochim. Acta*, 2008, **53**, 7131–7137.

41 Y. Xiao, H. X. Ju and H. Y. Chen, *Anal. Biochem.*, 2000, **278**, 22–28.
42 H. S. Yin, S. Y. Ai, W. J. Shi and L. S. Zhu, *Sens. Actuators, B*, 2009, **137**, 747–753.
43 B. Wang, J. J. Zhang, Z. Y. Pan, X. Q. Tao and H. S. Wang, *Biosens. Bioelectron.*, 2009, **24**, 1141–1145.
44 F. H. Wu, J. J. Xu, Y. Tian, Z. C. Hu, L. W. Wang, Y. Z. Xian and L. T. Jin, *Biosens. Bioelectron.*, 2008, **24**, 198–203.
45 X. S. Yang, X. Chen, L. Yang and W. S. Yang, *Bioelectrochemistry*, 2008, **74**, 90–95.
46 C. X. Lei, S. Q. Hu, N. Gao, G. L. Shen and R. Q. Yu, *Bioelectrochemistry*, 2004, **65**, 33–39.
47 X. D. Zeng, X. F. Li, X. Y. Liu, Y. Liu, S. L. Luo, B. Kong, S. L. Yang and W. Z. Wei, *Biosens. Bioelectron.*, 2009, **25**, 896–900.
48 W. J. Li, R. Yuan, Y. Q. Chai, L. Zhou, S. H. Chen and N. Li, *J. Biochem. Biophys. Methods*, 2008, **70**, 830–837.
49 C. H. Liu, X. L. Guo, H. T. Cui and R. Yuan, *J. Mol. Catal. B: Enzym.*, 2009, **60**, 151–156.
50 B. Q. Wang and S. J. Dong, *Talanta*, 2000, **51**, 565–572.
51 H. J. Chen and S. J. Dong, *Biosens. Bioelectron.*, 2007, **22**, 1811–1815.
52 A. K. M. Kafi, G. Wu and A. Chen, *Biosens. Bioelectron.*, 2008, **24**, 566–571.
53 Z. X. Cao, J. Zhang, J. L. Zeng, L. X. Sun, F. Xu, Z. Cao, L. Zhang and D. W. Yang, *Talanta*, 2009, **77**, 943–947.
54 R. Snyderman and E. J. Fundman, *J. Immunol.*, 1980, **124**, 2754–2757.
55 Y. Yoshioka, T. Kitao, T. Kishino, A. Yamamuro and S. Maeda, *J. Immunol.*, 2006, **176**, 4675–4681.